RSC Advances

PAPER

View Article Online
View Journal | View Issue

Cite this: *RSC Adv.*, 2025, **15**, 37263

Synthesis, characterization and bioactivity of chalcone-based polybenzoxazine/copper oxide nanocomposites

Hamada S. A. Mandour, * Ahmed Rehab, Mohamed Elnahrawy and Nehal Salahuddin

In the current work, a chalcone-based benzoxazine monomer was synthesized by Mannich condensation reaction using octadecylamine, paraformaldehyde, and a hydroxylated chalcone in a co-solvent of toluene/ethanol. The resulting benzoxazine monomer was mixed with nanoparticles of copper oxide at different ratios to obtain polybenzoxazine/copper oxide nanocomposites. The structure of the benzoxazine monomer was verified using FTIR and ^{1}H NMR, while the structure of polybenzoxazine/copper oxide nanocomposites was investigated using FTIR and XRD. The morphology of the resultant composites was examined using SEM and TEM. The thermal properties of polybenzoxazine/copper oxide nanocomposites were studied using TGA. The resulting composites were tested for antibacterial activity against some bacteria such as *E. coli*, *Pseudomonas aeruginosa*, *S. aureus*, and *Bacillus subtilis*. Also, the cytotoxic activity of the resulting materials was tested against some human cells like Mammary gland breast cancer (MCF-7), hepatocellular carcinoma (HEPG-2), human prostate cancer (PC-3), and colorectal carcinoma colon cancer (HCT-116). The incorporation of nanoparticles of copper oxide into the polybenzoxazine matrix enhanced the thermal stability, increased the char yield, and improved the bioactivity of benzoxazines. The bio-efficiency of these materials increased as the ratio of copper oxide in the composites was increased.

Received 8th July 2025
Accepted 1st October 2025

DOI: 10.1039/d5ra04893a

rsc.li/rsc-advances

1 Introduction

Despite many years of application history, phenolic resins are still important materials in polymer science. Traditional phenolic resins are widely used in electronics, aerospace, and other industries due to their good heat and chemical resistance, dimensional stability, low flammability, and electrical insulation. Among these attractive properties, they have some shortcomings, such as brittleness, the necessity of using acid or base catalysts, and the generation of by-products during curing, which causes some industrial and environmental problems.

Cope and Holly[1] created benzoxazine, a type of phenolic resin, for the first time in the 1940s by employing the Mannich condensation reaction of *ortho*-hydroxybenzylamine with formaldehyde in a solvent of water and benzene. In 1949, Burke[2] suggested a new method for benzoxazine synthesis using three main components: phenols, amines, and formaldehyde in 1 : 1 : 2 molar ratios. After that, this method was considered a general way to prepare benzoxazine due to its simplicity and ability to use many different raw materials. Other desirable properties of benzoxazines that are not found in phenolic resins include near-zero shrinkage cure, a high char yield, no release of by-products during the curing process, low water absorption, no strong acid catalyst required for curing, and long shelf life.[3] The most interesting and unique characteristic of this class of polymers is their extraordinarily rich molecular design flexibility, which allows the design of a variety of molecular structures to tailor the desired properties. Based on these features, polybenzoxazines (PBz) are ideal materials for replacing traditional phenolic resins in high-performance fields. However, some properties, such as their brittleness and low reactivity, which require high temperatures to achieve efficient polymerization, are still the main obstacles restricting the applications of benzoxazines.[4] Many studies of benzoxazine focused on designing new benzoxazine structures by incorporating different functional groups to expand their potential for applications. Many groups can be adopted onto the benzene of benzoxazine by using functional groups, such as alkenyl, halogenic, nitro, aldehyde, cyano, carboxyl, and maleimide.[5–11] In recent years, considerable efforts have been made to improve the toughness, flexibility, and other features of polybenzoxazines such as incorporating elastomeric polymers like polyurethane[12] and polysiloxane[13] into the thermosetting matrix or synthesizing composites of polybenzoxazine with other inorganic materials.[14–17]

Because of their excellent properties and numerous uses, copper oxide nanoparticles (CuONPs) are among the most

Chemistry Department, Faculty of Science, Polymer Research Group, Tanta University, Tanta 31527, Egypt. E-mail: Hamada.mandour@science.tanta.edu.eg

promising materials. CuONPs have excellent thermal stability, electrical conductivity, and bioreactivity. Copper oxide has several uses including catalysis,[18,19] gas sensors[20,21] superconductors[22] and bio-applications.[23,24] CuONPs have been synthesized using a variety of techniques including the sol–gel method,[25] electrochemical technique,[26] hydrothermal treatment,[27] spray pyrolysis,[28] sonochemical technique,[29] and microwave-assisted synthesis.[30]

To enhance the thermal conductivity of polybenzoxazine, a filler of boron nitride and copper particles was assembled with benzoxazine composites by Y. Wang *et al.*[31] 25% wt of this filler reached the thermal conductivity of PBz to 1.049 w m^{-1} k^{-1}, while using a high loading of filler cause a degradation in the mechanical properties of benzoxazine. X. Chen *et al.* used different coatings of cardanol-based benzoxazine and polyimide cardanol-based benzoxazine composite to protect the surface of copper metal from corrosion.[32] These coatings possessed good mechanical properties and excellent anti-corrosion performance. J. Chen *et al.* used urushiol-based benoxazine copper polymer as a marine antifouling coating.[33] The resulted materials have low surface energy, strong substrate adhesion, and excellent antibacterial activity towards Gram-negative bacteria (*E. coli*) and Gram-positive bacteria (*S. aureus*). N. Salahuddin *et al.* prepared benzoxazine monomer from a reaction of aniline, paraformaldehyde and a chalcone, then mixed it with different ratios of graphene oxide (GO) to obtain polybenzoxazine/GO composites.[34] The prepared composites have higher thermal stability and electrical conductivity compared to the pristine benzoxazine. The GO acts as a catalyst that reduced the curing temperature needed for benzoxazine polymerization.

Recently, there has been a lot of interest in nanomaterials (NPs), including carbon nanotubes (CNTs), nanometals (such as Ag, Au, Cu), nanometal oxides (such as MgO, ZnO, TiO_2, CuO), and their composites with antibacterial characteristics. Because of their special properties, which include a large surface area and high reactivity, nanomaterials can be used for applications in biofields. The characteristics of NPs and their antimicrobial activity can be influenced by their size, composition, structure, shape, concentration, surface characteristics, and environmental factors (like temperature, PH). Mendes *et al.* used ZnO NPs as antibacterial agents against the bacteria of *Staphylococcus aureus*, *Escherichia coli*, and *Pseudomonas aeruginosa*.[35] It was reported that the high efficiency of ZnO was related to the production of Zn^{2+} ions and the generation of reactive oxygen species (ROS). Abinaya and Kavitha prepared MgO NPs by four methods; sol–gel, microwave, hydrothermal, and green synthesis.[36] The antibacterial activity of MgO NPs was tested against bacteria of *S. aureus*, *E. coli*, *K. pneumonia*, and *E. faecalis*. The hydrothermal method of MgO NPs led to smaller particle size (29.5 nm) and exhibited higher bio-efficiency compared to the other ways. In many fields of technology, medicine, and agriculture, TiO_2 NPs are already in use. Serov *et al.* studied the synthesis methods of TiO_2 NPs, the physical and chemical properties, antimicrobial properties and the different factors that affect this activity.[37] The highest antimicrobial of TiO_2 NPs was obtained by amorphous morphology and a small particle size of 20–60 nm. The various efforts of using silver nanoparticles (AgNPs) as antimicrobial agents were investigated by Rodrigues *et al.*[38] Chuangang *et al.* reported the different mechanisms of antibacterial action of AgNPs, including rupture of cell membrane permeability, interference of bacterial DNA replication, and disruptions to cellular processes such as protein synthesis and respiration.[39] AgNPs damage microbial cells by releasing Ag^+ ions and Ag free radicals.[40] According to Sathiyaraj *et al.* the gold nanoparticles (AuNPs) have good antibacterial activity against both Gram-positive and Gram-negative bacteria.[41] The activity was related to the production of (ROS) or heat that can destroy the cells of bacteria.[42] Using copper oxide as an antibacterial towards a range of bacteria[43–46] and as an anticancer against different human cells[47–52] was studied. The mechanistic pathways of bioactivity of copper oxide were discussed by S. Meghana *et al.*[53]

This research aims to create innovative polybenzoxazine nanocomposites with copper oxide at various ratios, investigate their thermal stability, and study the bioactivity of these materials, such as their antibacterial and cytotoxic effects. To the best of your knowledge, this is the first study concerned with the preparation of composites of polybenzoxazine (prepared using chalcones) and nanoparticles of copper oxide to create new materials with improved properties and used them in new applications such as bio-fields. Synthesis of benzoxazine using chalcones is a way to expand the diversity of monomers and reduce the use of traditional phenols.

2 Experimental

2.1. Chemicals

4-Hydroxybenzaldehyde (LOBA-Chemie, India), copper acetate monohydrate, paraformaldehyde (Merck, Germany), stearyl amine, acetophenone (ADWIC-Egypt), sodium hydroxide (Bio-Chem for laboratory fine chemicals), toluene (NaTco. Laboratory chemicals reagent), oleic acid (Qualikems-India), 1,4-dioxane (S.D Fine-Chem Limited-India), glacial acetic acid (Diachem. Chemical), hydrochloric acid (ADWIC-Egypt), diethyl ether (S. D Fine-Chem Limited-India), dimethyl sulfoxide, and ethanol (Bio.Chem, Egypt) were used without further purification.

2.2. Preparation of copper oxide nanoparticles (CuONPs)

Copper oxide nanoparticles were synthesized by the aqueous precipitation method using copper(II) acetate as a precursor and sodium hydroxide as a reducing agent as follows:[54] in a 500 ml-round flask, 1.197 g (5.99 mmol) of copper acetate monohydrate [$Cu(CH_3COO)_2 \cdot H_2O$] was dissolved in 300 ml of distilled water with continuous stirring at room temperature for 30 minutes. 1 ml of glacial acetic acid (CH_3COOH) was added to the solution. 4 g (0.1 mol) of sodium hydroxide dissolved in 100 ml of distilled water was added dropwise to the solution till pH reached 11. A dark black precipitate of copper oxide appeared quickly when the solution was gradually warmed to 40 °C. For 24 hours, the solution was allowed to stir, then the precipitate was centrifuged for 5 minutes at 2500 rpm, and washed with

ethanol before being rinsed with distilled water. After drying in the oven at 60 °C for 48 hours, the yield was 0.55 g (46%).

2.3. Preparation of chalcone (3-(4-hydroxyphenyl)-1-phenylprop-2-en-1-one) (Cha)

Chalcones have been synthesized by the base-catalyzed Claisen–Schmidt condensation reaction of substituted acetophenones and aldehydes with an equimolar ratio (1 : 1) in the presence of alcoholic alkali.[55,56] A mixture of 4-hydroxybenzaldehyde (1.22 g, 0.01 mol) and acetophenone (1.2 g, 0.01 mol) was dissolved in 50 ml of ethanol in a 250 ml round-bottomed flask equipped with a magnetic stirrer. Then, 10 ml of NaOH solution (20% conc.) was added dropwise to the reaction mixture with vigorous stirring at room temperature. After 48 hours, the reaction mixture was neutralized with HCl (0.2 M), whereby the precipitation occurred. The precipitate was then dried at 60 °C for 48 hours to obtain 0.6 g (25%) of the chalcone (**Cha**).

2.4. Synthesis of benzoxazine monomer (Bm) and polybenzoxazine (PBm)

Stearyl amine 1.347 g (5 mmol), 1.12 g (5 mmol) of (**Cha**), and 0.3 g (10 mmol) of paraformaldehyde were mixed in 120 ml of a co-solvent of toluene/ethanol at a ratio of 1 : 1 (V/V). The reaction was refluxed at 110 °C with stirring for 48 hours. Diethyl ether was used to precipitate the benzoxazine monomer, which was then washed with sodium hydroxide, ethanol, and distilled water several times to eliminate any unreacted components. The precipitate was dried at 70 °C for 48 hours to obtain 1.5 g (58%) of benzoxazine monomer (**Bm**) Scheme 1. The polymerization of benzoxazine monomer was performed using a thermal curing process without catalysts. The thermal curing of (**Bm**) was carried out at 230 °C for two hours to afford polybenzoxazine (**PBm**) through ring-opening polymerization as shown in Scheme 1.

2.5. Synthesis of polybenzoxazine/copper oxide nanocomposites

0.475 g of benzoxazine monomer (**Bm**) was dissolved in 15 ml of 1,4-dioxane. 0.025 g of copper oxide nanoparticles (**CuONPs**) was added to the benzoxazine solution. Followed by adding 2 ml of oleic acid to the mixture and sonicating for 30 minutes at 40 °C. After that, the solvent was evaporated at 70 °C, and the resulting material was cured thermally at 230 °C to obtain **PBm/CuONP-5** (Scheme 1). The same procedure was performed using (0.45 g, 0.425 g) of (**Bm**) and (0.05 g, 0.075 g) of **CuONPs** to obtain (**PBm/CuONP-10**) and (**PBm/CuONP-15**), respectively.

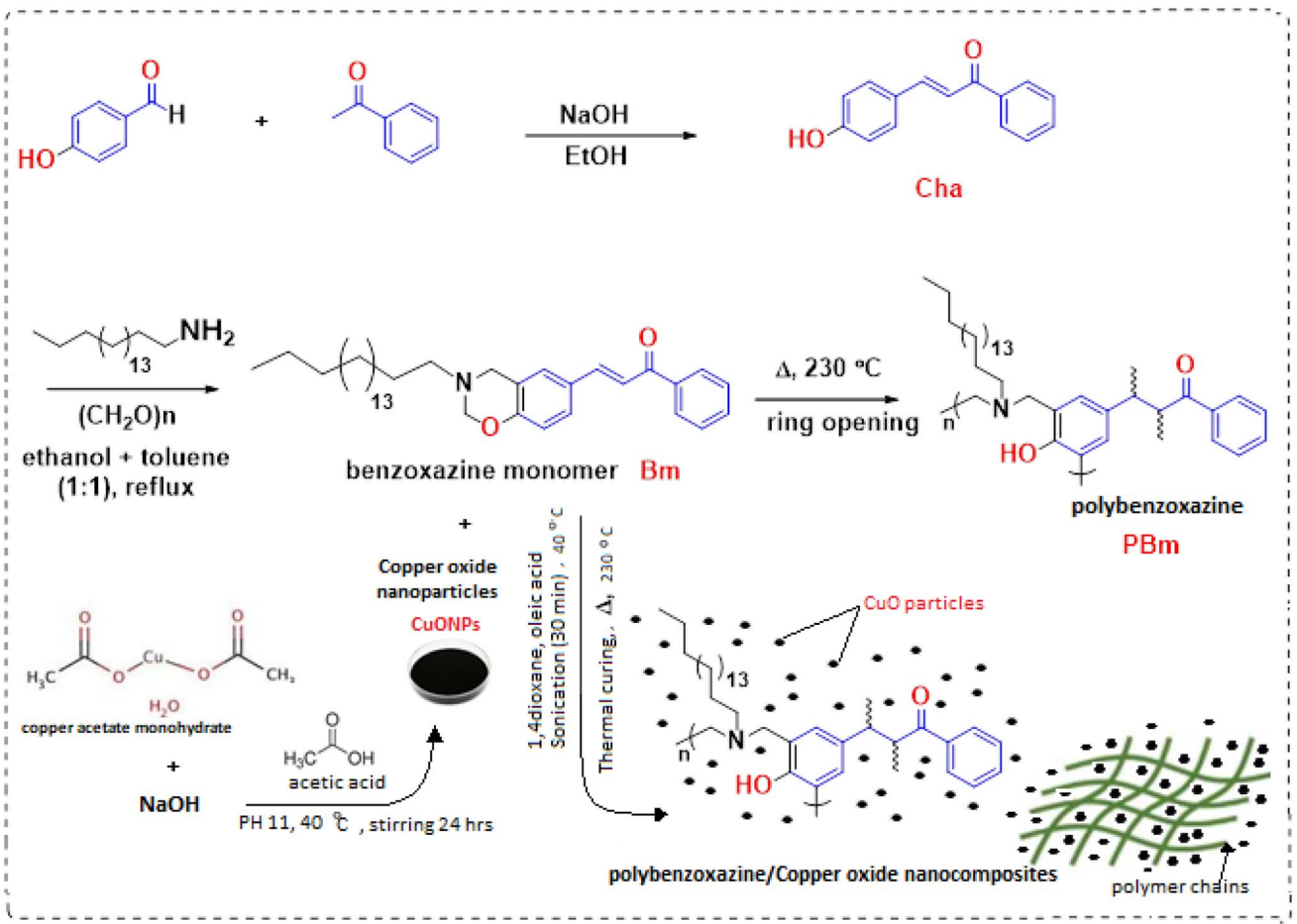

Scheme 1 Synthesis of benzoxazine monomer **Bm**, polybenzoxazine **PBm** and **PBm/CuO** nanocomposite.

2.6. Bioactivity tests

2.6.1. Antibacterial activity. The antibacterial activity of the synthesized compounds was tested against a panel of two Gram-positive bacteria (*Staphylococcus aureus*, *Bacillus subtilis*) and two Gram-negative bacteria (*Escherichia coli*, *Pseudomonas aeruginosa*). Each of the compounds was dissolved in a solvent of dimethyl sulfoxide (DMSO), and solutions with a concentration of 1 mg ml^{-1} were prepared separately. Paper discs of Whatman filter paper were prepared with a standard size (5 cm) and sterilized in an autoclave. The paper discs were soaked in the desired concentration of the complex solution and placed aseptically in the Petri dishes with nutrient agar media (agar 20 g + peptone 5 g + beef extract 3 g) seeded with *Staphylococcus aureus*, *Bacillus subtilis*, *E. coli*, and *Pseudomonas aeruginosa*. The Petri dishes were incubated at 36 °C, and the inhibition zones were recorded after 24 hours of incubation. Each treatment was replicated three times. The antibacterial activity of a common standard antibiotic ciprofloxacin was also recorded using the same procedure as above at the same concentration and solvents.[57] The activity index (%) for the complex was calculated using the following formula:

$$\%\ \text{Activity index} = \frac{\text{zone of inhibition by test compound (diametre)}}{\text{zone of inhibition by standard (diametre)}} \times 100 \quad (1)$$

2.6.2. Cytotoxicity assay

2.6.2.1. Cell line and reagents. The polybenzoxazine composites were tested as cytotoxic materials against the human cells of hepatocellular carcinoma (HEPG-2), mammary gland breast cancer (MCF-7), colorectal carcinoma colon cancer (HCT-116), and human prostate cancer (PC-3). The cell lines were obtained from ATCC *via* Holding company for biological products and vaccines (VACSERA), Cairo, Egypt. Doxorubicin was used as a standard anticancer drug for comparison. The reagents are RPMI-1640 medium, MTT, and DMSO (Sigma Co., St. Louis, USA), Fetal Bovine serum (GIBCO, UK).

2.6.2.2. MTT assay. The MTT test was utilized to assess the drugs inhibitory effects on cell growth using the aforementioned cell lines.[58] The basis of this colorimetric assay is the fact that mitochondrial succinate dehydrogenase in living cells transforms yellow tetrazolium bromide (MTT) into a purple formazan derivative. Cell lines were cultured in RPMI-1640 medium with 10% fetal bovine serum. Antibiotics added were 100 units per ml penicillin and 100 μg per ml streptomycin at 37 °C in a 5% CO_2 incubator. The cell lines were seeded in a 96-well plate at a density of (1.0×10^4) cells per well at 37 °C for 48 hours under 5% CO_2. After incubation, the cells were treated with different concentrations of compounds and incubated for 24 hours. After 24 hours of drug treatment, 20 μl of MTT solution at 5 mg ml^{-1} was added and incubated for 4 hours. To dissolve the purple formazan that forms, 100 ml of dimethyl sulfoxide (DMSO) is poured into each well. A plate reader (EXL 800, USA) is used to measure and record the colorimetric test at an absorbance of 570 nm. The relative cell viability in percentage was calculated as follows:

$$(A570 \text{ of treated samples}/A570 \text{ of untreated sample}) \times 100 \quad (2)$$

3 Methods

Nuclear magnetic resonance ^{1}H NMR spectra were obtained by means of a Bruker at 400 MHz using $CDCl_3$ as a solvent. Fourier transform infrared (FTIR) absorption spectra were performed using a PerkinElmer 1420 spectrometer with a frequency range from 4000 to 400 cm^{-1} using a potassium bromide disk with 64 scans. X-ray diffraction (XRD) was observed using an X-ray diffractometer GRN, APD 2000 PROXRD, using Cu-K_a radiation ($\lambda = 1.5418$ Å) and voltage (40 kV) at a scale of 4°–90° in scanning speed of 0.03 min^{-1}. The surface morphology of the nanocomposite was characterized by scanning electron microscope (SEM, SU8000, Hitachi Ltd), with accelerating voltage 25 kV, landing voltage 2.0 kV, DW (4.0 mm). The internal morphology of nanocomposites was investigated using a transmission electron microscope (TEM, JEOL-JEM100-IDO-SX, JEOL Ltd, Japan) with an accelerating voltage of 20 kV. TGA thermograms were determined using a Shimadzu -TGA-50H thermal analyzer system in the temperature range of 30–800 °C under a nitrogen atmosphere with heating at 20 °C min^{-1} and a gas flow rate of 40 ml min^{-1}. The ultrasonic device used was Hunmanlab-Ultrasonic cleaner (50/60 Hz, 60 w, Korea). The centrifuge device used was (mlw T5, EBMLW, Germany) with 8 sample holders.

4 Results and discussion

4.1. ^{1}H NMR

Hydrogen proton nuclear magnetic resonance ^{1}H NMR was used to determine the structure of the benzoxazine monomer. ^{1}H NMR spectrum of (**Bm**) was as follows: (400 MHz, $CDCl_3$) reveals δ 0.87 (t, 3H) corresponding to the methyl group from stearyl amine, 1.25 (s, 32H) corresponding to the sixteen methylene groups from stearyl amine, 2.73 (t, 2H) corresponding to the last methylene group from stearyl amine, 4.02 (s, 2H) corresponding to the methylene group far from oxygen in oxazine ring, 4.92 (s, 2H) corresponding to the methylene group between oxygen and nitrogen in the oxazine ring, 6.79 (d, 1H), 7.27 (s, 1H), 7.37 (d, 1H), 7.45 (dd, 1H), 7.49 (d, 2H), 7.56–7.59 (m, 1H), 7.72 (d, 1H), 7.99–8.02 (m, 2H) corresponding to the aromatic protons in the benzoxazine monomer.

4.2. FTIR

To identify the structures and functional groups of the prepared materials, we used fourier transform infrared analysis (FTIR). The structures of benzoxazine monomer, polybenzoxazine, copper oxide nanoparticles, and benzoxazine/copper oxide nanocomposites at various ratios were investigated as shown in Fig. 1(a and b). The spectrum of benzoxazine **Bm** (Fig. 1a) revealed the absorption peaks at 1017 cm^{-1} and 1237 cm^{-1} which are due to the C–O–C symmetric and asymmetric stretching modes of the oxazine ring, respectively. The peak that appeared at 1169 cm^{-1} corresponds to C–N–C asymmetric stretching of the oxazine ring. The bands that appeared at 935 cm^{-1} and 1500 cm^{-1} correspond to a tri-substituted benzene ring. During the ring-opening polymerization, the closed oxazine rings have been consumed, and each oxazine

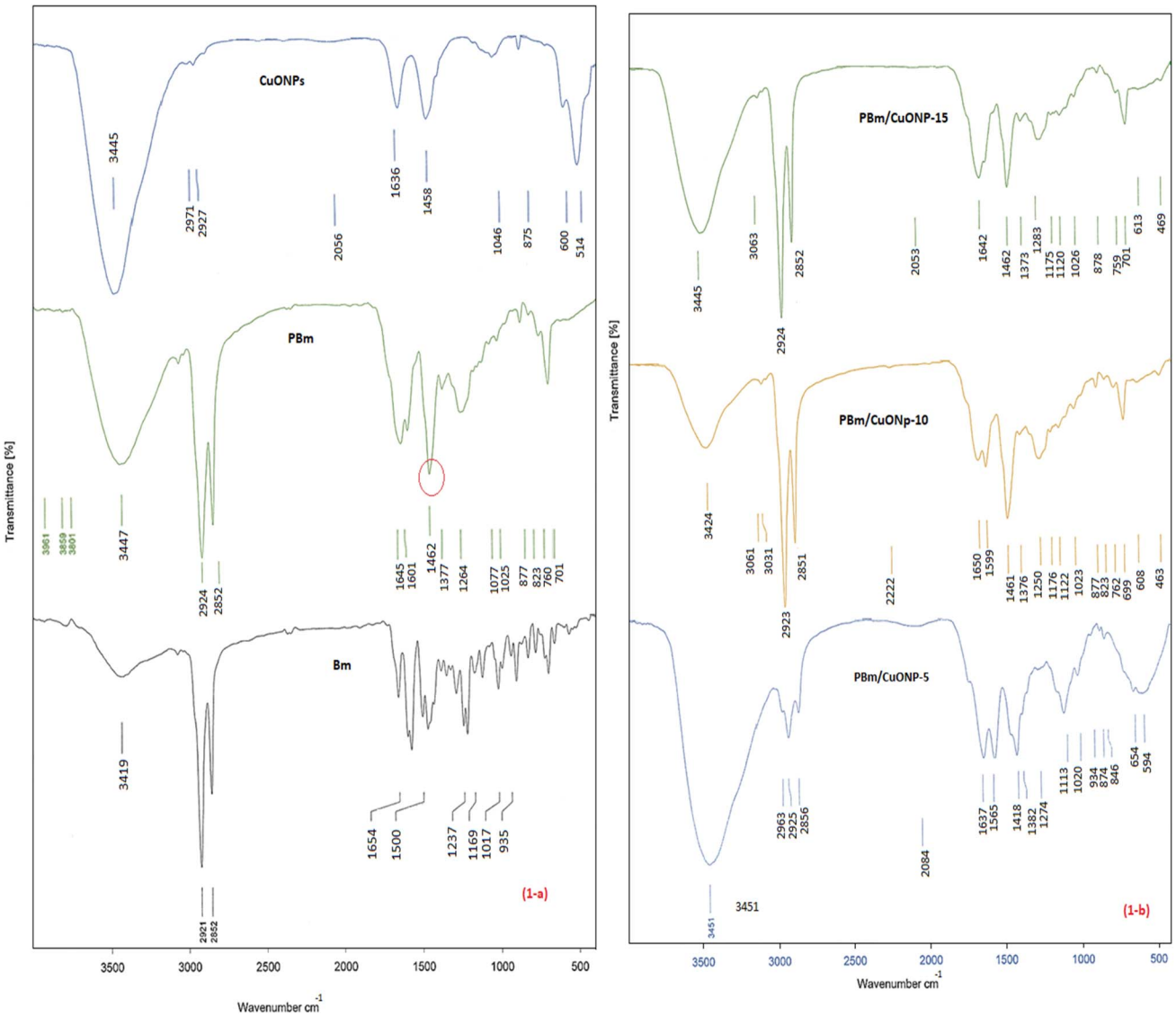

Fig. 1 (a) FTIR of benzoxazine monomer **Bm**, polybenzoxazine **PBm**, copper oxide nanoparticles and (b) nanocomposites of benzoxazine/CuO at different ratios.

ring leads to phenolic O–H formation. The spectrum of **PBm** (Fig. 1a) reveals a broad phenolic hydroxyl characteristic absorption peak at 3447 cm^{-1}. The oxazine ring of benzoxazine has a distorted structure between oxygen and nitrogen, above and below the benzene ring plane. Due to their high basicity, both oxygen and nitrogen in the oxazine ring can act as potential sites of polymerization initiation, increasing the strain around the ring and making it more suitable to open.[59] With the completion of ring-opening polymerization, the tri-substituted bands at 935 cm^{-1} and 1500 cm^{-1} disappeared, and a new absorption peak appeared at 1462 cm^{-1}, which is ascribed to the tetra-substituted benzene ring.[60] The FTIR spectrum of **CuONPs** (Fig. 1a) shows peaks at 514 cm^{-1} and 600 cm^{-1} due to the formation of the monoclinic phase of pure copper oxide, which are assigned to the stretching vibrations of the Cu–O bond.[61,62] The absorption band observed at 1636 cm^{-1} is related to O–H bending vibration. The broad peak centered at 3445 cm^{-1} is attributed to the stretching vibrations of absorbed water molecules. The characteristic bands of polybenzoxazine and copper oxide appeared for **PBm/CuO** nanocomposites at various ratios with modest changes in their positions (Fig. 1b).

4.3. XRD

To identify the crystallinity structure of the prepared materials based on their diffraction patterns, we used X-ray diffraction (XRD) analysis. Fig. 2 shows the XRD patterns of **PBm**, **CuONPs**, and **PBm/CuO** nanocomposites at different contents of copper oxide. The XRD of CuO nanoparticles shows the peaks at 2θ around (32°, 35°, 38°, 48°, 52°, 59°, 62°, 66°, 68°, 72°, and 76°), which are related to the planes of (110), (002), (111), (202), (020), (202), (113), (022), (113), (311) and (222), respectively, that show the monoclinic phase of the CuO nanoparticles.[53,63] The sharp peaks of CuO are related to its crystalline structure, while the

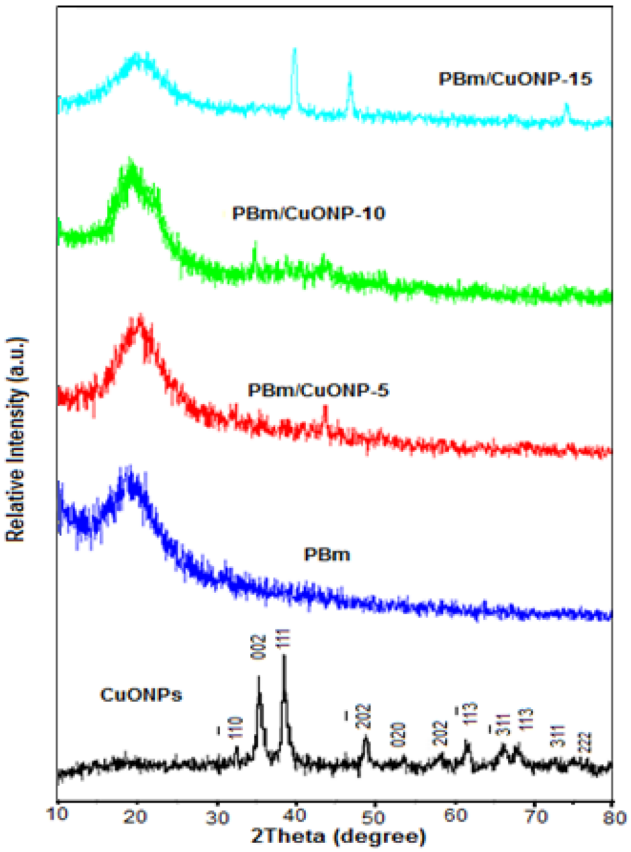

Fig. 2 XRD of copper oxide nanoparticles **CuONPs**, polybenzoxazine **PBm**, and **PBm/CuO** nanocomposites.

broad peak near to 20° of **PBm** is due to its amorphous structure. The crystallite size was 13.4 nm, as determined by the Scherrer equation;

$$(D = k\lambda/\beta \cos\theta) \quad (3)$$

where D is the particle diameter size, K is Scherrer's constant (shape factor, 0.94), λ is the wavelength of X-ray source (1.541 Å), β is the full width at half-maximum (FWHM), and θ is the diffraction angle corresponding to the lattice plane. The crystallite size of **CuONPs** was measured at $2\theta = 38°$ (111), which considered the major intensity peak of copper oxide. For **PBm/CuO** nanocomposites, the characteristic peaks of copper oxide seem weak, especially with a small content of inorganic matter, and then become slightly clearer with an increase in the amount of dispersed phase.

4.4. SEM

To examine the surface morphology of composites, we used the scanning electron microscope technique. Fig. 3(a and b) shows the SEM images of (**PBm/CuONP-15**) at different magnifications. The SEM image at high magnification (10 000×) showed a degree of homogenous distribution of the composite components with no phase boundaries and minimal aggregations suggesting a well-mixed composite material. The surface of the composite appears to have a berry-like structure and also, doesn't appear smooth or soft, but it seems to have a degree of roughness.

4.5. TEM

Transmission electron microscopy was used to investigate the internal morphology, microstructure, shape, and particle size of the materials. The TEM images of (**PBm/CuONP-15**) are shown in Fig. 4 at different magnifications. The particles observed in the micrographs are nearly spherical or quasi-spherical in shape. Furthermore, a relatively homogenous distribution was observed with few aggregations. The average particle size of the CuO nanoparticles was found to be 15.3 nm, which agrees well with the Scherrer equation measured using XRD.

4.6. TGA

The thermal properties of the resulted materials were studied using thermal gravimetric analysis (TGA). Fig. 5 showed the TGA thermograms of polybenzoxazine (**PBm**) and **PBm/CuONP** composites at various ratios of copper oxide content. It was noticed that adding of CuO nanoparticles to the polymer matrix of polybenzoxazine improved the thermal stability of the prepared materials. Due to the CuO insertion in the polymer, the residual weight of (**PBm/CuONP-15**) was close to 50% at 600 °C. The char yield was also increased from 20.2% of the pristine polymer **PBm** to reach 23.85%, 28%, and 33.1% for (**PBm/CuONP-5**, **PBm/CuONP-10**, and **PBm/CuONP-15**),

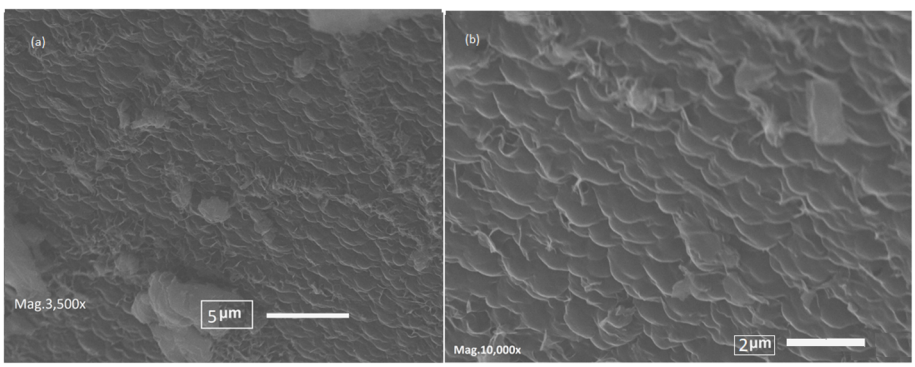

Fig. 3 SEM images of **PBm/CuO-15** nanocomposite; (a) at low magnification (3500×) and (b) at high magnification (10 000×).

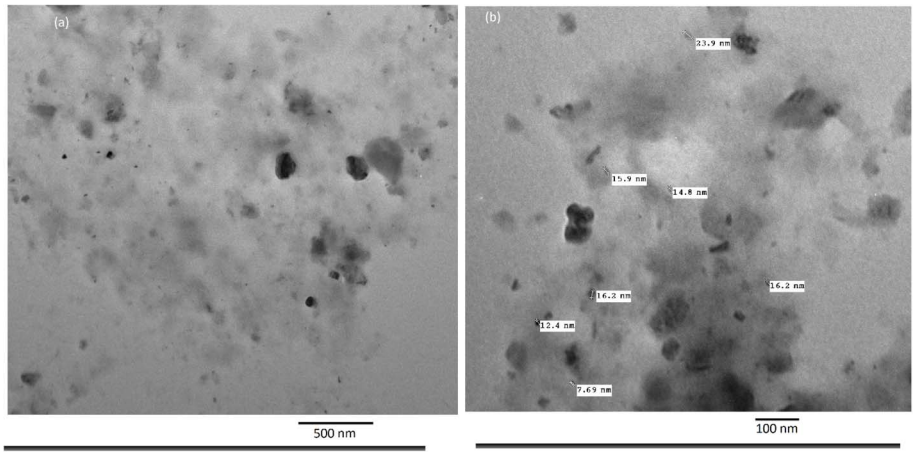

Fig. 4 TEM images of PBm/CuO-15 nanocomposite; (a) at magnification of 10 000× and (b) at magnification of 30 000×.

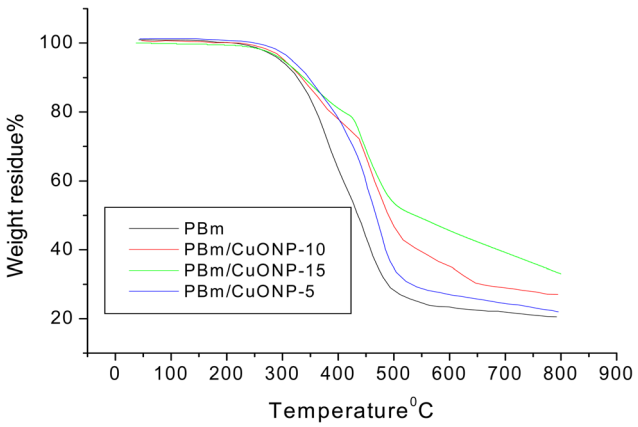

Fig. 5 TGA of polybenzoxazine PBm and PBm/CuO nanocomposites.

Table 1 The weight loss of PBm and PBm/CuO NP-15 at different temperatures

Temperature (°C)	(PBm) weight loss %	(PBm/CuO NP-15) weight loss %
200	0.6	0.58
300	4.4	4.72
400	24.4	19.8
500	66.2	46.02
600	73.7	54.34
700	76.4	60.8
725	77.13	62.3
750	78.08	63.9
775	78.84	65.43
Char yield % (at 800 °C)	20.2	33.1

respectively. Table 1 shows the weight loss of **PBm** and **PBm/CuONP-15** at temperatures ranging from 200 to 800 °C. At a temperature of 400 °C, the weight loss of (**PBm** and **PBm/CuONP-15**) was 24.4% and 19.8%, respectively. At a temperature of 700 °C, the weight loss of (**PBm** and **PBm/CuONP-15**) was 76.4% and 60.8%, respectively. The presence of CuO as a dispersed material in the bulk phase of polybenzoxazine can restrict polymer chains movement and slow down the degradation process. Moreover, the presence of CuO in the polybenzoxazine chains may increase the hydrogen bonding (due to the presence of O–H groups on its surface) and crosslinking density, resulting in an improvement of the thermal properties.

4.7. Biological applications

4.7.1. Anti-bacterial activity. The US Environmental Protection Agency (EPA) has designated elemental copper and its derivatives as antimicrobial materials.[64] When copper oxides are reduced to nanoscale, their antibacterial action against pathogenic microbes is increased. This makes copper oxides suitable for use commercially in different fields like textiles, paints, agriculture, and healthcare. The antibacterial activities of copper oxide, polybenzoxazine **PBm**, and **PBm/CuONP** composites at various concentrations are mentioned in Table 2. The antibacterial activities of these materials were studied against the microorganisms of *E. coli*, *Pseudomonas aeruginosa* (Gram-positive bacteria), *S. aureus*, and *Bacillus subtilis* (Gram-negative bacteria). The results showed that **CuONPs** have good activity against the four types of microorganisms, especially *Pseudomonas aeruginosa* and *S. aureus*. For polybenzoxazine, it was noticed that **PBm** has no bio-effect on these organisms. For **PBm/CuO** nanocomposites, antibacterial properties were observed towards the studied organisms and theses bioactivities were related to the presence of CuO in the composites. **PBm/CuO** nanocomposites had different efficiencies against the tested bacteria. For **PBm/CuONP-5** with low content of copper oxide, the resulted composite has a bio-effect only on the bacteria of *S. aureus*. With increasing the amounts of copper oxide, the antibacterial effect of **PBm/CuoNP-10** and **PBm/CuONP-15** improved against the different bacteria, such as *Pseudomonas aeruginosa* and *S. aureus*.

Due to the small size of CuO NPs, they have a high surface area compared to their volume. So, they are able to enter and interact with the cell surface of bacteria. With accumulation on the membrane cell, gaps were created in the integrity of the

Table 2 Antibacterial activities of CuONPs, PBm, and PBm/CuONP at different ratios of copper oxide

	E. coli		*Pseudomonas aeuroginosa*		*S. aureus*		*Bacillus subtilis*	
Compound	Diameter of inhibition zone (mm)	% Activity index	Diameter of inhibition zone (mm)	% Activity index	Diameter of inhibition zone (mm)	% Activity index	Diameter of inhibition zone (mm)	% Activity index
CuONP	11	47.8	17	80.9	15	75	13	56.5
PBm	NA	—	NA	—	NA	—	NA	—
PBm-CuONP-5	NA	—	NA	—	5	25	NA	—
PBm-CuONP-10	2	8.7	9	42.8	7	35	8	34.8
PBm-CuONP-15	6	26.1	10	47.6	9	45	10	43.5

bilayer, leading to the cell membrane not being able to regulate the movement of substances in and out of the cell. This may lead to the entry of materials that are not vital for the cell and the exit of others that may be necessary. The cell membrane is semipermeable, but with interaction with the nano-copper oxide it becomes more permeable, causing the damage of its intercellular structures and the death of the cell with time. When copper oxide penetrates the cell, they interact with its components and induce the release of reactive oxygen species (ROS), forming free radicals and cationic copper. The copper ions can bind to negatively charged nucleic acid protein, causing structural deformation of the bacteria cell. Copper ions can interact with various electron donor functional groups like phosphates, thiols, hydroxyls, imidazoles, and indoles. According to Ma *et al.*, the discharge of copper ions affects the stability of cell membrane and metabolic processes.[65] The copper oxide may interfere with the bacterial replication processes by sticking to nucleic acids. As a result of interaction with the genetic material of the bacteria cell, the ribosome may be denatured, resulting in suppression of protein synthesis, translation, and transcription. According to Ameh *et al.* the antibacterial activity of CuO NPs was related to inducing oxidative stress and DNA damage with the microorganisms.[66] To be effective as agents, NPs must reach the pathogens. NPs interact with pathogens *via* van der Waals electrostatics, hydrophobic/hydrophilic interactions, and receptor-ligand binding.[67,68] Modi *et al.* reported that smaller NPs have the ability to release more metal ions, interact with bacteria cells more readily, dissolve more quickly, and more ROS.[69] According to Zarchi *et al.* nanometals and nanometals oxides are able to inhibit pathogens by generation of ROS.[70] After entering the cell, NPs can do so by phagocytosis, pinocytosis, and other forms of endocytosis, including clathrin-mediated and caveolin-mediated endocytosis.[71,72] According to Meghana *et al.* the antibacterial activity of copper oxide is due to the formation of free radicals or reactive oxygen species (ROS), a sharp fall in cell membrane integrity leading to disruption of cell function, affecting protein synthesis and DNA structure, damage to the fumarase enzyme of bacteria, and cell death.[53] Also, it was though that the rough nature of the composite's surface (as it appears from SEM) can increase the binding and interfere with the body of microorganisms.

4.7.2. Cytotoxic activity. The cytotoxic impacts of polybenzoxazin/copper oxide nanocomposites against the following human cells: mammary gland breast cancer (MCF-7), hepatocellular carcinoma (HEPG-2), human prostate cancer (PC-3), and colorectal carcinoma colon cancer (HCT-116) were studied. For comparison, doxorubicin, a common anticancer drug, was used. The results of cytotoxic activities of **CuONPs**, **PBm**, and **PBm/CuONP** composites at different concentrations were mentioned in Table 3. The viability of cancer cells against **PBm/CuONPs** exposure was performed by MTT assay (3-(4,5-dimethyl-2-triazolyl-2,5-diphenyl-2-tetrazolium bromide)) as mentioned by Mossman.[58] Cytotoxic activities of compounds were evaluated by the half-minimal inhibitory concentration (IC_{50}). MTT results showed that copper oxide significantly decreased the viability of all tested cells. The results showed that **CuONPs** has a very strong effect against HePG2, HCT-116, MCF-7 PC3 and a strong effect against PC3. For polybenzoxazine, **PBm** has a weak effect against most of the tested cells. For polybenzoxazine/copper oxide nanocomposites, it was noticed that all concentrations have different effects on the tested cells, and this effect increased with an increase in the amount of copper oxide in the composite. For example, **PBm/CuONP-15** has a strong cytotoxic effect against MCF-7 and a moderate effect against HePG2 and HCT-116. According to M. Shafag *et al.* CuONPs exerted distinct impaction on cell viability *via* selective killing of cancer cells and its cytotoxicity against chronic myeloid leukemia was through the generation of reactive oxygen species (ROS).[73] R. Mahmood *et al.* reported that the

Table 3 The cytotoxic effects of PBz/CuO nanoparticles against different cells

	In vitro cytotoxicity IC_{50}[a] (μM)			
Compounds	HePG2	HCT-116	MCF-7	PC3
Dox [b]	4.50 ± 0.2	5.23 ± 0.3	4.17 ± 0.2	8.87 ± 0.6
CuONP	7.26 ± 0.5	10.49 ± 0.9	6.48 ± 0.4	14.53 ± 1.2
PBz-f-Th	63.76 ± 3.1	85.51 ± 4.2	87.43 ± 4.3	>100
PBZ-f/CuONP-5	46.34 ± 2.6	72.64 ± 3.5	56.72 ± 3.2	75.95 ± 3.9
PBZ-f-CuONP-10	39.02 ± 2.4	45.62 ± 2.5	26.41 ± 2.2	66.21 ± 3.5
PBZ-f-CuONP-15	23.79 ± 1.8	33.87 ± 2.3	19.10 ± 1.5	41.08 ± 2.8

[a] IC_{50} (μM): 1–10 (very strong). 11–20 (strong). 21–50 (moderate). 51–100 (weak) and above 100 (non-cytotoxic). [b] **Dox:** doxorubicin.

strong cytotoxicity of CuONPs towards the breast cancer cell line was due to cell membrane destruction causing cellular enzymes.[47] H. Fahmy *et al.* mentioned that the cytotoxicity of CuONPs against lung carcinoma cells was related to the generation of (ROS) which comes from free radicals such as hydroxyl radicals, superoxide, peroxides, and the damage of DNA of the cells.[48] V. Gnanavel *et al.* studied the cytotoxic effect of CuONPs for colon cancer cell lines and found that the efficiency of copper oxide was related to the ROS process, which led to cell membrane defects and DNA damage of the cells.[49] According to Ivask *et al.* the hydroxyl radical is a very reactive oxygen radical that can react very quickly with almost every type of molecules found in the living cells.[74] The combination of two hydroxyl radicals leads to hydrogen peroxide formation.

5 Conclusion

A benzoxazine monomer was prepared from a hydroxylated chalcone with long chains of aliphatic amine (stearyl amine) and paraformaldehyde using the Mannich reaction. The polybenzoxazine was prepared by ring-opening polymerization of the monomer. The resulting benzoxazine monomer was mixed with nanoparticles of copper oxide in various weights followed by thermal polymerization to obtain polybenzoxazine/copper oxide nanocomposites. SEM images showed a rough surface with a homogenous distribution of particles on the surface. The particle size of CuO was measured using TEM to be 15.3 nm. The incorporation of copper oxide into the polymer matrix of benzoxazine had improved its thermal stability and the char yield, such as from 20.2% for the pristine polymer to 23.85%, 28% and 33.1% for **PBm/CuONP-5**, **PBm/CuONP-10**, and **PBm/CuONP-15**, respectively. Due to the incorporation of copper oxide, the resulting polybenzoxazine composites had bioactivity features, such as using **PBm/CuONP-10** and **PBm/CuONP-15** as antibacterial against *S. aureus* and *Bacillus subtilis*. Also, the prepared composites had a good cytotoxic effect against some human cells, such as using **PBm/CuONP-10** against MCf-7 and HePG2 or using **PBm/CuONP-15** against HePG2, HCT-116, MCF-7 and PC3. Generally, with increasing the amounts of copper oxide in the benzoxazine composites, the bioactivity enhanced.

6 Future work

From the results that were obtained, we think that there are numbers of the future trends or work that may be built upon this research, such as (1). Synthesis of excess benzoxazine monomers that have some functional groups that though they have a biological effect, particularly the chalcones which have high biological efficiency. (2) Use these monomers with CuO or other nano-metals or nano-metal oxides as microbial agents for different bacteria, fungi, and viruses. (3) The presence of copper oxide into the composites can make coatings that render the adhesion and growth of microorganisms, so we think it will be a good application that needs to further work. (4) Polybenzoxazines are insulator materials, so we think the incorporation of conducting material into the matrix as copper oxide can acquire it a suitable electric conductivity, and this can lead to an excess of applications of benzoxazine in a new area.

Conflicts of interest

There are no conflicts to declare.

Data availability

The data that support this study are available by request.

Supplementary information is available. See DOI: **https://doi.org/10.1039/d5ra04893a**.

References

1 F. W. Holly and A. C. Cope, *J. Am. Chem. Soc.*, 1944, **66**, 1875.
2 W. J. Burke, *J. Am. Chem. Soc.*, 1949, **71**, 609.
3 H. Ishida, T. Agag, *Handbook of Benzoxazine Resins*, Elsevier, 2011.
4 T. Takeichi, Y. Guo and S. Rimdusit, *Polymer*, 2005, **46**, 4909.
5 T. Agag and T. Takeichi, *Macromole*, 2003, **36**, 6010.
6 P. Velez-Herrera, H. Ishida and J. Fluor, *Chem*, 2009, **130**, 573.
7 R. Andreu, J. A. Reina and J. C. Ronda, *J. Polym. Sci., Part A:Polym. Chem.*, 2008, **46**, 3353.
8 Q. Ran, Q. Tian, C. Li and Y. Gu, *Polym. Adv. Technol.*, 2010, **21**, 170.
9 H. Qi, H. Ren, G. Pan, Y. Zhuang, F. Huang and L. Du, *Polym. Adv. Technol.*, 2009, **20**, 268.
10 R. Mahfud, T. Agag, H. Ishida, S. Shaikh and S. Qutubuddin, *J. Colloid Interface Sci.*, 2013, **407**, 339.
11 H. Ishida and S. Ohba, *Polymer*, 2005, **46**, 5588.
12 S. Rimdusit, M. Sudjidjune, C. Jubsilp and S. Tiptipakorn, *J. Appl. Polym. Sci.*, 2014, **131**(13), 40502.
13 T. Takeichi, T. Agag and R. Zeidam, *J. Polym. Sci., Part A:Polym. Chem.*, 2001, **39**, 2633.
14 K. D. Demir, M. A. Tasdelen, T. Uyar, A. W. Kawaguchi, A. Sudo, T. Endo and Y. Yagci, *J. Polym. Sci., Part A:Polym. Chem.*, 2011, **49**, 4213.
15 F. Meng, H. Ishida and X. Liu, *RSC Adv.*, 2014, **4**, 9471.
16 K. S. Santhosh Kumar, C. P. Reghunadhan Nair and K. N. Ninan, *J. Appl. Polym. Sci.*, 2008, **107**, 1091.
17 B. Kiskan, A. L. Demirel, O. Kamer and Y. Yagci, *J. Polym. Sci., Part A:Polym. Chem.*, 2008, **46**, 6780.
18 R. Karimian and F. Piri, *J. Nanostruct. Chem.*, 2013, **3**, 87.
19 K. Zhang, J. M. Suh, T. H. Lee, J. H. Cha, J.-W. Choi, H. W. Jang, R. S. Varma and M. Shokouhimehr, *Nano Convergence*, 2019, **6**, 1.
20 Y. Li, J. Liang, Z. Tao and J. Chen, *Mater. Res. Bull.*, 2008, **43**, 2380.
21 T. Ishihara, M. Higuchi, T. Takagi, M. Ito, H. Nishiguchi and Y. Takita, *J. Mater. Chem.*, 1998, **8**, 2037.
22 G. Malandrino, A. Frassica, G. G. Condorelli, G. Lanza and I. L. Fragalà, *J. Alloys Compd.*, 1997, **251**, 314.
23 S. Nations, M. Long, M. Wages, J. D. Maul, C. W. Theodorakis and G. P. Cobb, *Chemosphere*, 2015, **135**, 166.

24 F. Perreault, S. P. Melegari, C. H. da Costa, A. L. de, O. F. Rossetto, R. Popovic and W. G. Matias, *Sci. Total Environ.*, 2012, **441**, 117.
25 K. Nithya, P. Yuvasree, N. Neelakandeswari, N. Rajasekaran, K. Uthayarani, M. Chitra and S. S. Kumar, *Int. J. ChemTech Res.*, 2014, **6**, 2220.
26 F. Parveen, B. Sannakki, M. V Mandke and H. M. Pathan, *Sol. Energy Mater. Sol. Cells*, 2016, **144**, 371.
27 K. J. Arun, A. K. Batra, A. Krishna, K. Bhat, M. D. Aggarwal and P. J. J. Francis, *Am. J. Mater. Sci.*, 2015, **5**, 36.
28 A. Moumen, B. Hartiti, P. Thevenin and M. Siadat, *Opt. Quantum Electron.*, 2017, **49**, 1.
29 C. Karunakaran, G. Manikandan and P. Gomathisankar, *J. Alloys Compd.*, 2013, **580**, 570.
30 H. A. Elazab, *Biointerface Res. Appl. Chem.*, 2018, **8**, 3278.
31 Y. Wang, N. Wu, D. Drummer, C. Liu, W. Shen, F. Tomiak, K. Schneider, X. Liu and Q. Chen, *J. Mater. Des*, 2020, **191**, 108698.
32 X. Chen, X. Zhang, J. Chen, W. Bai, X. Zhang, Q. Lin, Q. Lin, F. Lin and Y. Xu, *RSC Adv.*, 2022, **12**, 10766.
33 J. Chen, W. Bai, B. Zheng, Y. Xu, R. Jian, C. Huang, F. Wei, K. Yang, Y. Lin and Q. Lin, *J. Cleaner Prod.*, 2021, **318**, 128527.
34 N. Salahuddin, A. Rehab, I. Y. El-Deep and R. Elmokadem, *Polym. Bull.*, 2022, **79**, 3175.
35 C. Mendes, G. Dillari, C. Forsan, V. Sapata, P. Lopes, P. Moraes, R. Motagnolli, H. Ferreira and E. Bidoia, *Sci. Rep.*, 2022, **12**, 2658.
36 S. Abinaya and H. Kavitha, *ACS Omega*, 2023, **8**, 52255.
37 D. Serov, A. Gritsaeva, F. Yanbaev, A. Simakin and S. Gudkov, *Int. J. Mol. Sci.*, 2024, **25**, 10519.
38 A. Rodrigues, J. Batista, M. Rodrigues, V. Thipe, L. Minarini, P. Lopes and A. Lugao, *Front. Microbiol.*, 2024, **31**, 15.
39 Y. Chuangang, C. Han, X. Wang, Y. Zheng, Q. Li, X. Hu and H. Sun, *Mol. Biol. Rep.*, 2012, **39**, 9193.
40 M. Abbasi, R. Gholizadeh, S. Kasaee, A. Vaez, S. Chelliapan and F. Fadhil, *Sci. Rep.*, 2023, **13**, 5987.
41 S. Sathiyaraj, G. Suriyakala, A. Gandhi, R. Babujanarthanam, K. Almaary, T. Chen and K. Kaviyarasu, *J. Infect. Public Health.*, 2021, **14**, 1842.
42 M. Okkeh, N. Bloise, E. Restivo, L. De Vita, P. Pallavicini and L. Visai, *J. Nanomater.*, 2021, **11**, 312.
43 S. Jadhav, S. Gaikwad, M. Nimse and A. Rajbhoj, *J. Cluster Sci.*, 2011, **22**, 121.
44 S. Sagadevan, S. Vennila, A. Marlinda, Y. Al-Douri, M. Johan and J. Anita, *Appl. Phys. A:Mater. Sci. Process.*, 2019, **125**, 489.
45 A. Khalaji, Z. Pazhand, K. Kiani, P. Machek, M. Jarosova and R. Mazandarani, *J. Mater. Sci.: Mater. Electron.*, 2020, **31**, 11949.
46 A. Khalaji, M. Soleymainfard, M. Jarosova and P. Machek, *J. Invest. Surg.*, 2020, **14**, 961.
47 R. Mahmood, A. Kadhim, S. Ibraheem, S. Albukhaty, H. Salih, R. Abbas, M. Jabeir, *et al.*, *Sci. Rep.*, 2022, **12**, 16165.
48 H. Fahmy, N. Ebrahim and M. Gaber, *J. Trace Elem. Med. Biol.*, 2020, **60**, 126481.
49 V. Gnanavel, V. Palanichamy and S. Roopan, *J. Photochem. Photobiol., B*, 2017, **171**, 133.
50 S. Shide, S. Parjane, H. Turakane, P. Basnet, R. Oza, Y. Abhale, S. Pansambal, *et al.*, *J. Sol-Gel Sci. Technol.*, 2023, **106**, 737.
51 T. Revathi and S. Thambidurai, *Int. J. Biol. Macromol.*, 2019, **139**, 867.
52 Y. Cao, H. Dhahad, M. El-Shorbagy, H. Alijjani, M. Zakeri, A. Heydari, E. Bahonar, *et al.*, *Sci. Rep.*, 2021, **11**, 23479.
53 S. Meghana, P. Kabra, S. Chakraborty and N. Padmavathy, *RSC Adv.*, 2015, **5**, 12293.
54 M. Ahamed, H. A. Alhadlaq, M. A. M. Khan, P. Karuppiah and N. A. Al-Dhabi, *J. Nanomater.*, 2014, **2014**, 637858.
55 A. L. Choudhary and V. Juyal, *Int. J. Pharm. Pharm. Sci.*, 2011, **3**, 125.
56 M. Attarde, A. Vora, A. Varghese and Y. Kachwala, *Org. Chem.: Indian J.*, 2014, **10**, 192.
57 A. Stylianakis, N. Kolocouris, G. Kolocouris, B. Fytas, E. Foscolos, J. Padalko, D. Neyts, *et al.*, *Bioorg. Med. Chem. Lett*, 2003, **13**, 1699.
58 T. Mosmann, *J. Immunol. Methods*, 1983, **65**, 55.
59 Y. Yagci, B. Kiskan and N. N. Ghosh, *J. Polym. Sci., Part A:Polym. Chem.*, 2009, **47**, 5565.
60 S. Gârea, H. Iovu, A. Nicolescu and C. Deleanu, *Polym. Test.*, 2007, **26**, 162.
61 M. T. Baig and A. Kayan, *Mater. Res. Bull.*, 2024, **180**, 113070.
62 A. A. Radhakrishnan and B. B. Beena, *Indian J. Adv. Chem. Sci.*, 2014, **2**, 158.
63 M. P. Neupane, Y. K. Kim, I. S. Park, K. A. Kim, M. H. Lee and T. S. Bae, *Surf. Interface Anal.*, 2009, **41**, 259.
64 L. Arendsen, R. Thakar and A. sultan, *Clin. Microbiol. Rev.*, 2019, **32**, 4.
65 X. Ma, A. Zhou, X. Xu and Q. Du, *Front. Surg.*, 2022, **9**, 905892.
66 T. Ameh, M. Gibb, D. Stevens, S. Pradhan, E. Braswell and C. Sayes, *Nanomater*, 2022, **12**, 2402.
67 W. Gao, S. thamphiwatana, P. Angsantikul and L. Zhang, *Wiley Interdiscip. Rev.:Nanomed. Nanobiotechnol.*, 2024, **6**, 532–547.
68 B. Iuan, T. Huynh and R. Zhou, *Nanoscale*, 2016, **8**, 5750–5754.
69 S. Modi, K. Inwati, A. Gacem, S. Saquib, R. Prajapat, K. Yadav, *et al.*, *Antibiotics*, 2022, **11**, 708.
70 H. Zarchi, S. Sagharchi, N. Sepahdoost, M. Jamalabadi, J. Gross, H. Jooya and A. Samadi, *Adv. Biomed. Res.*, 2024, **13**, 113.
71 S. Behzadi, V. Serpooshan, W. Tao, M. A. Hamaly, Y. Alkawareek, E. Dreaden, *et al.*, *Chem. Soc. Rev.*, 2017, **46**, 4218–4244.
72 G. Sahay and Y. A. V. Kabanov, *J. Controlled Release*, 2010, **145**, 182–195.
73 M. Shafagh, F. Rahmani and N. Delirezh, *Iran. J. Basic Med. Sci.*, 2015, **10**, 993.
74 A. Ivask, O. Bondarenko, N. Jepihhina and A. Kahru, *Anal. Bioanal. Chem.*, 2010, **398**, 701.